Collision-induced photon echo at the transition 0 ↔ 1 in ytterbium vapor: Direct proof of depolarizing collision anisotropy

N. N. Rubtsova,* V. G. Gol'dort, V. N. Ishchenko, E. B. Khvorostov, and S. A. Kochubei
A. V. Rzhanov Institute of Semiconductor Physics, Siberian Branch of the Russian Academy of Sciences, 13 Academician Lavrentyev Avenue, Novosibirsk 630090, Russia

V. A. Reshetov
Togliatti State University, 14 Belorusskaya Street, Togliatti 445667, Russia

I. V. Yevseyev
Moscow Physical Engineering State Institute, 31 Kashirskoye Shosse, Moscow 115409, Russia
(Received 19 April 2011; published 14 September 2011)

A collision-induced photon echo arising at the transition 0 ↔ 1 of ytterbium in the presence of heavy atomic buffer is investigated. Collision-induced echo signal appears in the case of mutually orthogonal linear polarizations of exciting pulses and it is absent without buffer. Collision-induced echo power grows with buffer pressure up to the maximum value and decays exponentially at further buffer pressure growth. Collision-induced echo power is essentially less than that of the ordinary echo generated by pulses with parallel polarizations in the same mixture, and its polarization is linear with the polarization vector directed along that of the first exciting pulse. All the properties of collision-induced photon echo are explained on the basis of collision relaxation dependence on the direction of active atom velocity.

DOI: 10.1103/PhysRevA.84.033413 PACS number(s): 42.50.Md, 34.10.+x

I. INTRODUCTION

Photon echo is the most known phenomenon among numerous coherent transients. After the first experiment in a solid [1], the prediction of photon echoes in gases [2,3], and the first photon-echo observation in molecular gas [4], photon echo became of great importance in basic and applied research. Today the applications of photon echo concern the structure and dynamics of macromolecules [5], high-resolution spectroscopy of solids [6], local vibrations in disordered solids [7], and other fundamental research [8–10]. Photon echo generated by shaped femtosecond pulses of tunable radiation is one of the most promising tools for the investigation of ultrafast relaxation in condensed media [11]. Photon-echo applications for quantum memory [12,13] and for echo-based optical processors [14,15] seem to be very topical.

Photon echo in gases allowed us to understand a lot of fine details of collision relaxation in atoms and in molecules. In particular, inelastic collisions in molecular gases [16], depolarizing collisions in molecular [17] and in atomic gases [18], and the possibility to select the slow molecules [19] were investigated by photon-echo technique.

One of the most simple quantum transitions of type 0 ↔ 1 realized at the inter-combination transition $(6s^2)\,^1S_0 \leftrightarrow (6s6p)\,^3P_1$ of ^{174}Yb attracted attention of many experimental research groups as an ideal quantum system (without hyperfine structure of atomic levels) [20–23]. Optical data storage and readout [20], non-Faraday rotation of photon-echo polarization in a weak magnetic field [24], and different aspects of atomic collisions were investigated using quantum transitions between lower energy levels of ^{174}Yb [21,22].

In this paper we focused our attention on the detailed investigation of a new phenomenon—collision-induced photon echo at the transition 0 ↔ 1—which appears exclusively due to anisotropy of depolarizing collisions, that is, due to relaxation matrix dependence on the direction of active atom velocity.

II. VELOCITY DEPENDENCE AND ANISOTROPY OF COLLISION RELAXATION

Collision (pressure) broadening is extremely important for molecular transitions in the microwave and infrared regions. Corresponding cross sections and collision decay rates Γ were calculated on the basis of the isotropic model, taking into account the transitions between quantum states of molecules caused by collisions [25,26]. A simple model of the interaction potential $V \propto 1/r^n$ with $n \geqslant 3$ (here r is the distance between active atom and buffer particle) used in [27] (see also references) was presented in order to explain the results concerning velocity dependence of collision decay rate $\Gamma(v)$ measured by photon echo generated in $^{13}CH_3F$ gas via level Stark switching in the presence of saturating cw laser radiation. The traditional method of photon-echo generation was used in [28] to study $\Gamma(v)$ dependence in gas SF_6 and in its mixture with Kr. This approach allowed us [28] to confirm the exchange mechanism of rotation relaxation in the gas of nonpolar molecules SF_6 and it made evident the contribution of short-range forces in collision relaxation to a SF_6-Kr mixture.

As compared to vibrorotation transitions in the infrared spectral range, the atomic transitions in a visible spectral range are more sensitive to radiation decay of working levels, phase-interrupting collisions, and depolarizing collisions; the last relaxation channel seems to be dominating in spectral

*rubtsova@isp.nsc.ru

line broadening of intercombination transition $(6s^2)\,^1S_0 \leftrightarrow (6s6p)\,^3P_1$ of ^{174}Yb in our experimental conditions.

The anisotropy of collision relaxation becomes evident when analyzing the collision relaxation of active (radiating) atom surrounded by a gas of heavy atomic buffer particles. Indeed, in the frame system of the active particle moving at velocity $\mathbf{v}$, the collision picture acquires the axial symmetry with an axis along the vector $\mathbf{v}$; the active atom experiences the action of the flow of buffer particles moving at the drift velocity $-\mathbf{v}$. This visual picture was named in [29] "the wind effect." In [29] the theory accounting for the anisotropic collisions is constructed for the spectral line pressure broadening of transitions between degenerate levels, and the analysis of factors preventing experimental observation of anisotropy is made. There was a great number of theoretical predictions related to collision relaxation anisotropy (see, for example, [29–33] and references therein) for different spectroscopic problems including absorption or Raman scattering spectral line collision broadening and resonance fluorescence collision depolarization. In all cases, anisotropy of collision relaxation gives some small contribution to the line shape and broadening on the background of prevalent isotropic collision relaxation. A detailed analysis of depolarizing collisions including the dependence of relaxation matrices on atomic velocities was made in [34].

As for experimental verification, it was limited mainly to the prelaser era investigations of resonant fluorescence depolarization by collisions in atomic vapors [35] (the so-called hidden alignment in a gas discharge). Taking into account the difficulties preventing experimental investigations of collision relaxation anisotropy, it would be better to look for some phenomenon arising exclusively due to this effect. Such a prediction was made in [36] just for a collision-induced photon echo generated at the transition $0 \leftrightarrow 1$. Small angular momenta of working levels involved in this transition not only allow us to perform analytical calculations. Specific polarization properties of ordinary photon echo generated on the transition $0 \leftrightarrow 1$ permit finding experimental conditions for which the contribution of anisotropic depolarizing collisions implies a new phenomenon.

III. POLARIZATION PROPERTIES OF ORDINARY PHOTON ECHO IN YTTERBIUM VAPOR AT TRANSITION $0 \leftrightarrow 1$

Polarization properties of photon echo generated in atomic gas at the transitions $0 \leftrightarrow 1$ and $1 \leftrightarrow 1$ were analyzed theoretically in [37]. Photon echo generated at such transitions by two pulses of resonant radiation with linear polarizations and polarization vectors making an angle ψ should have linear polarization. Echo polarization vector should be located along the polarization vector of the second exciting pulse. So, photon echo generated at these two types of transitions by linearly polarized exciting pulses "follows" the polarization of the second pulse. Its amplitude is proportional to $\cos(\psi)$; hence, for the angle $\psi = 90^\circ$, the photon echo should be absent. For exciting pulses of resonant radiation with circular polarizations, the ordinary photon echo appears only in case when both pulses have identical polarizations, either both right circular or both left circular ones. Exciting pulses of opposite circular polarizations do not generate photon echo at the transitions $0 \leftrightarrow 1$ and $1 \leftrightarrow 1$ [37].

So the photon echo at the transitions $0 \leftrightarrow 1$ and $1 \leftrightarrow 1$ in a pure gas should not appear either for exciting pulses of mutually orthogonal linear polarizations or for the pulses of opposite circular polarizations.

It is worth noting that polarization properties of photon echo generated in a gas at the transitions of type $0 \leftrightarrow 1$ or $1 \leftrightarrow 1$ have no dependence on the area of exciting radiation pulses. This property predicted in [37] makes the two above-mentioned transitions very attractive for experimental research.

Experimental research of polarization properties of photon echo generated at the intercombination transition $(6s^2)\,^1S_0 \leftrightarrow (6s6p)\,^3P_1$ of ^{174}Yb (transition of type $0 \leftrightarrow 1$) was, for the first time, performed in [38] for a complete set of polarizations of two exciting pulses of resonant radiation (linear-linear, circular-linear, linear-circular, and circular-circular) in a pure ytterbium vapor. The photon-echo polarization in pure ytterbium at the transition $0 \leftrightarrow 1$ coincides with the polarization of the second exciting pulse in all cases. In pure ytterbium vapor, the photon echo at the transition $0 \leftrightarrow 1$ did not appear either for exciting pulses of mutually orthogonal linear polarizations, or for the pulses of opposite circular polarizations, in agreement with the predictions [37].

This polarization property of ordinary photon echo generated in a gas at the transition of type $0 \leftrightarrow 1$ seems to be a key which allows us to look for the manifestation of depolarizing collisions anisotropy in preferential experimental conditions.

IV. THEORY OF COLLISION-INDUCED PHOTON ECHO AT TRANSITION $0 \leftrightarrow 1$

A. Photon-echo formation

Let us consider the photon-echo formation at the transition with the angular momentum change $J_a = 0 \rightarrow J_b = 1$ by two resonant laser pulses with durations T_1 and T_2, τ being the time interval between them. The electric field strength of these pulses, propagating along axis Z with carrier frequency ω, may be written as

$$\mathbf{E}_n = e_n \mathbf{l}_n \exp\{-i(\omega t - kz)\} + \text{c.c.}, \quad n = 1,2, \tag{1}$$

where e_n and $\mathbf{l}_n$ are the amplitudes and unit polarization vectors of the pulses. We consider the pulses to be much shorter than all the times of homogeneous relaxation. Then the dynamics of the atom under the action of nth laser pulse is governed by the equation for slowly varying atomic density matrix $\hat{\rho}$,

$$\dot{\hat{\rho}} = \frac{i}{2}[\hat{\Omega}_n, \hat{\rho}], \tag{2}$$

$$\hat{\Omega}_n = \Delta(\hat{P}_b - \hat{P}_a) + \frac{2|d|e_n}{\hbar}(\hat{g}_n + \hat{g}_n^\dagger). \tag{3}$$

Here $\Delta = kv_z - \omega + \omega_0$ is the frequency detuning from resonance, v_z is the Z component of the atomic velocity, $\hat{P}_{a,b}$ are the projectors on the subspaces corresponding to the atomic levels a and b, $d = d(J_a J_b)$ is the reduced matrix element of the electric dipole moment operator for the transition $J_a \rightarrow J_b$, while $\hat{g}_n = (\hat{\mathbf{g}}\mathbf{l}_n^*)$, where $\hat{\mathbf{g}}$ is the dimensionless electric dipole moment operator for the transition $J_a \rightarrow J_b$,

the matrix elements of its circular components being expressed through Wigner 3j symbols:

$$(\hat{g}_q)^{ab}_{m_a m_b} = (-1)^{J_a - m_a} \frac{d}{|d|} \begin{pmatrix} J_a & 1 & J_b \\ -m_a & q & m_b \end{pmatrix}. \quad (4)$$

The solution of Eq. (2) may be expressed through the evolution operator $\hat{S}_n$:

$$\hat{\rho}(T_n) = \hat{S}_n \hat{\rho}(0) \hat{S}_n^{\dagger}, \hat{S}_n = \exp\left(\frac{i}{2}\hat{\Omega}_n T_n\right), \quad (5)$$

where $\hat{\rho}(0)$ and $\hat{\rho}(T_n)$ are the atomic density matrices at some point z of the gaseous medium before and after the nth laser pulse passes through this point. The explicit expression for the evolution operator $\hat{S}_n$ is presented in Appendix A.

Initially the atom is at its ground state, its density matrix being $\hat{\rho}(0) = \hat{P}_a$. The first laser pulse creates atomic coherence on the transitions $m_a = 0 \to m_b = q = \pm 1$, which is described by the nondiagonal elements of the atomic density matrix

$$\rho^{ab}_{0q}(T_1) = (\hat{S}_1)^{aa}_{00} (\hat{S}_1^{\dagger})^{ab}_{0q}. \quad (6)$$

The evolution of these nondiagonal density matrix elements, which are responsible for the echo formation, in the time interval between the pulses is determined by the frequency detuning Δ, including Doppler shift kv_z, and by the irreversible relaxation. Here we take into account the two most rapid relaxation processes: the spontaneous radiation decay of the excited level, which is characterized by the relaxation rate $\gamma^{(1)}$, and the elastic depolarizing collisions, which do not change the atomic velocities but give rise to the transitions between various Zeeman sublevels of atomic resonant levels [39]. In case of transitions $J_a = 0 \to J_b = 1$ such collisions are characterized by two different complex relaxation rates, depending on the absolute value v of the atomic velocity—one $\Gamma_0(v) + i\Delta_0(v)$ for the dipole moment component collinear with the atomic velocity, the other $\Gamma_1(v) + i\Delta_1(v)$ for the dipole moment component perpendicular to the atomic velocity [36]—so that in the frame of reference, where the axis Z' is directed along the atomic velocity vector $\mathbf{v}$, the evolution of the atomic coherence $\rho'^{ab}_{0q}(T_1)$ is merely exponential. The equations describing the evolution of the matrix elements $\rho^{ab}_{0q}(T_1)$ in the original frame of reference, where the axis Z is directed along the wave vector of the laser pulses, may be obtained by means of rotation matrices (see Appendix B) and may be written as follows:

$$\rho^{ab}_{0q}(\tau) = e^{-\gamma\tau + i\delta\tau} \sum_{q'} R_{qq'}(\tau) \rho^{ab}_{0q'}(T_1), \quad (7)$$

where $\gamma = \gamma^{(1)} + [\Gamma_1(v) + \Gamma_0(v)]/2$ includes the average decay rate of atomic coherence due to elastic depolarizing collisions and $\delta = \Delta - [\Delta_1(v) + \Delta_0(v)]/2$ includes the average frequency shift of atomic coherence due to such collisions, while the relaxation matrix $R_{qq'}(\tau)$ is determined by the difference

$$\lambda(v) = \Gamma_0(v) - \Gamma_1(v) + i[\Delta_0(v) - \Delta_1(v)]$$

in two complex relaxation rates. The explicit expression for the relaxation matrix $R_{qq'}(\tau)$ is presented in Appendix B. This matrix depends on the atomic velocity vector $\mathbf{v}$. It depends on the velocity magnitude v only through its dependence on $\lambda(v)$, while its dependence on the velocity direction (spherical angles θ and ϕ of the velocity vector) is expressed explicitly through the rotation matrices.

In case of isotropic collision relaxation ($\lambda = 0$) the relaxation matrix is reduced to the unity matrix $[R_{qq'}(\tau) = \delta_{qq'}]$, while in case of anisotropic collision relaxation ($\lambda \neq 0$) the relaxation matrix $R_{qq'}(\tau)$ contains the nonzero nondiagonal elements $R_{-1,1}(\tau)$ and $R_{1,-1}(\tau)$ which describe the mutual transfer of coherence between the transitions $m_a = 0 \to m_b = -1$ and $m_a = 0 \to m_b = 1$ under the action of depolarizing collisions. Such transfer of coherence results in the spatial rotation of the atomic electric dipole moment vectors.

The second laser pulse reverses the Doppler dephasing according to the solution of Eq. (2):

$$\rho^{ab}_{0q}(T_2) = \sum_{q'} (\hat{S}_2)^{ab}_{0q'} \rho^{ba}_{q'0}(\tau) (\hat{S}_2^{\dagger})^{ab}_{0q} \sim e^{-i\delta\tau}. \quad (8)$$

After the passage of the second pulse through the medium the atomic evolution again is determined by the relaxation and is described by the equation similar to (7):

$$\rho^{ab}_{0q}(t') = e^{-\gamma t' + i\delta t'} \sum_{q'} R_{qq'}(t') \rho^{ab}_{0q'}(T_2), \quad (9)$$

where $t' = t - z/c - T_1 - \tau - T_2$.

The electric field strength of the echo signal,

$$\mathbf{E}^e = \mathbf{e}^e(t') \exp\{-i(\omega t - kz)\} + \text{c.c.},$$

is obtained from the Maxwell equations in a usual way:

$$\mathbf{e}^e(t') = 2\pi i\omega \frac{L}{c} n_0 |d| \int f(\mathbf{v}) d\mathbf{v} \text{Tr}\{\hat{\rho}(t')\hat{\mathbf{g}}\}, \quad (10)$$

where L is the length of the gaseous medium, n_0 is the concentration of resonant atoms, $f(\mathbf{v})$ is the Maxwell velocity distribution function, while the atomic density matrix $\hat{\rho}(t')$ at the instant of time t' is determined by (9). Vector $\mathbf{e}^e(t')$ may be presented as a sum of two components:

$$\mathbf{e}^e(t') = e^e_1(t')\mathbf{s}_1 + e^e_2(t')\mathbf{s}_2,$$

where $\mathbf{s}_n$ $(n = 1,2)$ are the two arbitrary unit orthogonal $(\mathbf{s}_n \mathbf{s}^*_m = \delta_{nm})$ vectors in the plane XY. We note that the density matrix $\hat{\rho}(t')$ in (9) depends on the atomic velocity vector $\mathbf{v}$ through the dependence on $\mathbf{v}$ of evolution operators $\hat{S}_n$ $(n = 1,2)$ and relaxation matrices $R_{qq'}(\tau)$ and $R_{qq'}(t')$, though we do not include $\mathbf{v}$ in the formal list of arguments of these functions for the formulas not to look too cumbersome.

Henceforth, we assume the dependence of the relaxation constants on the velocity magnitude v to be weak, so that

$$\Gamma_q(v) \approx \Gamma_q(u), \Delta_q(v) \approx \Delta_q(u),$$

where $u = \sqrt{2k_b T/m}$ is the atomic thermal velocity and the condition of the exact resonance $\omega = \omega_0 - (\Delta_0 + \Delta_1)/2$ to be fulfilled. We also neglect the irreversible relaxation in the course of the echo pulse, as well as it was neglected in the course of the exciting pulses, so that in the expression for $\hat{\rho}(t')$ in the right-hand side of Eq. (10) $\gamma t'$ and $\lambda t'$ may be replaced by $\gamma\tau$ and $\lambda\tau$. Then, after the successive substitution of Eqs. (6)–(9) in (10) with an account of the formulas for the matrix elements of the evolution operators (A4) and (A5)

we obtain for the two echo polarization components $e_n^e(t') = \mathbf{e}^e(t')\mathbf{s}_n^*$ the following expression:

$$e_n^e(t') = e_0 e^{-2\gamma\tau} \int f(\mathbf{v}) d\mathbf{v} e^{-iku_z(t'-\tau)} F(v_z) H_n, \qquad (11)$$

where $e_0 = \pi\omega L n_0 |d|/c\sqrt{3}$, $F(v_z)$ is defined by the chain of equations:

$$F(v_z) = \frac{\theta_1\theta_2^2}{\Omega_1 T_1 \Omega_2^2 T_2^2} Q_1 \sin^2\left(\frac{\Omega_2 T_2}{2}\right), \qquad (12)$$

$$Q_1 = \left[\sin(\Omega_1 T_1) + i\frac{kv_z}{\Omega_1}[1 - \cos(\Omega_1 T_1)]\right], \qquad (13)$$

$$\theta_n = \frac{2|d|e_n T_n}{\sqrt{3}\hbar}, \quad \Omega_n T_n = \sqrt{(kv_z T_n)^2 + \theta_n^2}, \qquad (14)$$

while

$$H_n = W(\mathbf{l}_2, \mathbf{l}_1) W^*(\mathbf{s}_n, \mathbf{l}_2). \qquad (15)$$

In Eq. (15) $W(\mathbf{a},\mathbf{b})$ denotes the scalar function of two vector arguments $\mathbf{a}$ and $\mathbf{b}$:

$$W(\mathbf{a},\mathbf{b}) = \mathbf{a}\hat{R}(\tau)\mathbf{b}^* = \sum_{q,q'} R_{qq'}(\tau) a_{-q} (b_{-q'})^*, \qquad (16)$$

where $R_{qq'}(\tau)$ are the elements of the relaxation matrix and a_q and b_q are the circular components of vectors $\mathbf{a}$ and $\mathbf{b}$.

The factor $F(v_z)$ contains the dependence of the echo amplitude on the areas θ_n (14) of the exciting pulses. This factor depends on the Z projection v_z of the atomic velocity through the dependence on v_z of Rabi frequencies Ω_n (14). In case of short exciting pulses ($kuT_n \ll 1$) $F(v_z)$ does not depend on v_z and provides a familiar echo dependence on the exciting pulse areas:

$$F(v_z) = \sin(\theta_1)\sin^2\left(\frac{\theta_2}{2}\right).$$

However, in the case of long exciting pulses ($kuT_n \gg 1$) the dependence of $F(v_z)$ on v_z becomes essential and determines the temporal shape and the duration of the echo pulse. Next, the factor H_n contains the dependence of the echo amplitude on the polarization vectors $\mathbf{l}_n$ of the exciting pulses and on the elements of relaxation matrix $\hat{R}(\tau)$. The factor H_n depends on the atomic velocity vector $\mathbf{v}$ through the dependence on $\mathbf{v}$ of relaxation matrix $\hat{R}(\tau)$.

B. Polarization properties of the collision-induced photon echo

We suppose that the difference $\lambda = \Gamma_0 + i\Delta_0 - \Gamma_1 - i\Delta_1$ in the two relaxation rates due to the elastic depolarizing collisions is much less than the homogeneous half-width γ of the spectral line, $|\lambda| \ll \gamma$, so that considering the ordinary echo we may assume the relaxation matrix to be just a unity matrix: $R_{qq'}(\tau) = \delta_{qq'}$. Then, as it follows from (15) and (16), factor H_n in Eq. (11) does not depend on the atomic velocity $\mathbf{v}$ and is given by the relation

$$H_n = (\mathbf{l}_2\mathbf{s}_n^*)(\mathbf{l}_2\mathbf{l}_1^*),$$

which means that the polarization of the ordinary echo coincides with that of the second exciting pulse, and the maximum echo amplitude is obtained with the similar polarizations of both exciting pulses. In particular, when both exciting pulses are linearly polarized along the axis X, the echo amplitude is determined by the following equations:

$$e_x^e(t') = e_0 e^{-2\gamma\tau} g(t'-\tau), e_y^e(t') = 0, \qquad (17)$$

where the function

$$g(t'-\tau) = \int_{-\infty}^{\infty} f(v_z) dv_z e^{-iku_z(t'-\tau)} F(v_z) \qquad (18)$$

describes the temporal shape of the ordinary echo pulse. Here $f(v_z)$ is the Maxwell distribution function in the Z projections of the atomic velocity, while factor $F(v_z)$ is determined by (12)–(14).

However, in case of orthogonal polarizations of the exciting pulses ($\mathbf{l}_2\mathbf{l}_1^* = 0$) the two signals formed on the transitions $m_a = 0 \to m_b = -1$ and $m_a = 0 \to m_b = 1$ interfere destructively, so that the ordinary echo ultimately disappears. The echo signal in this case appears only due to the action of elastic depolarizing collisions, which cause the transfer of coherence between different magnetic substates of resonant levels and are described by the nondiagonal elements of the relaxation matrix $\hat{R}(\tau)$. In the general case of orthogonal elliptic polarizations the Cartesian axes X and Y may be directed along the axes of polarization ellipses of the exciting pulses so that the circular components of the two polarization vectors $\mathbf{l}_n$ may be determined by the only one real parameter α:

$$l_{1,q} = \cos(\alpha)\delta_{q,-1} - \sin(\alpha)\delta_{q,1}, \qquad (19)$$

$$l_{2,q} = \sin(\alpha)\delta_{q,-1} + \cos(\alpha)\delta_{q,1}. \qquad (20)$$

This parameter α defines the ratio of the lengths $a_n^{(x)}$ and $a_n^{(y)}$ of the the axes of polarization ellipse of the nth pulse along the axes X and Y according to the relation

$$\left|\tan\left(\alpha - \frac{\pi}{4}\right)\right| = \frac{a_1^{(y)}}{a_1^{(x)}} = \frac{a_2^{(x)}}{a_2^{(y)}},$$

while the sign of $\tan(\alpha - \pi/4)$ determines the direction of rotation of the pulse electric field vector in the plane XY: If $\tan(\alpha - \pi/4) > 0$, then the first pulse is polarized left elliptically and the second pulse is polarized right elliptically, and vice versa; if $\tan(\alpha - \pi/4) < 0$, then the first pulse is polarized right elliptically and the second pulse is polarized left elliptically. The particular value $\alpha = 0$ corresponds to the circular orthogonal polarizations: the first pulse right-circularly polarized $l_{1,q} = \delta_{q,-1}$, the second one left-circularly polarized $l_{2,q} = \delta_{q,1}$. The particular value $\alpha = \pi/4$ corresponds to the linear orthogonal polarizations: the first pulse polarized along the axis X, the second one along the axis Y.

Since the two polarization vectors defined by (19) and (20) are orthonormal we may choose them as the basis vectors $\mathbf{s}_n$ in the plane XY. Then factor H_n in Eq. (11) becomes

$$H_n = W(\mathbf{l}_2, \mathbf{l}_1) W^*(\mathbf{l}_n, \mathbf{l}_2),$$

where function $W(\mathbf{a},\mathbf{b})$ is defined by (16). After the substitution in (16) of the circular components (19) and (20) of vectors $\mathbf{l}_n$ and of the elements of relaxation matrix $R_{qq'}(\tau)$ defined by Eqs. (B7) and (B8) of Appendix B, we obtain the explicit dependence of factor H_n on the spherical angles θ and ϕ of the atomic velocity vector $\mathbf{v}$. As the dependence of the relaxation

matrix elements $R_{qq'}(\tau)$ on the angle ϕ is determined simply by the exponential factors (B7):

$$R_{qq'}(\tau) \sim e^{i(q'-q)\phi},$$

then the integral over this angle ϕ on the right side of Eq. (11) is easily calculated. After such integration the two components $e_n^c(t')$ of the electric field strength of the collision-induced photon echo become as follows:

$$e_n^c(t') = \frac{e_0}{2} e^{-2\gamma\tau} \left| \sinh\left(\frac{\lambda\tau}{2}\right) \right|^2 \sin(2\alpha) g_c(t'-\tau) l_n^c, \quad (21)$$

where the unit vector $\mathbf{l}^c$ with the components

$$l_1^c = -\sin(2\alpha), l_2^c = \cos(2\alpha) \quad (22)$$

describes the polarization of the collision-induced echo, while the function $g_c(t'-\tau)$ describes its temporal shape. The expression for this function contains the integrals over the velocity angle θ and over the velocity magnitude v:

$$g_c(t'-\tau) = \frac{2}{u^3\sqrt{\pi}} \int_0^\pi G(\theta, t'-\tau) \sin^5(\theta) d\theta, \quad (23)$$

$$G(\theta,t) = \int_0^\infty e^{-(v/u)^2 - ikvt\cos(\theta)} F[v\cos(\theta)] v^2 dv. \quad (24)$$

In Eq. (24) function $F[v\cos(\theta)] = F(v_z)$ is determined by (12)–(14) and u is the atomic thermal velocity.

As follows from (21), the intensity of the collision-induced echo depends on the ellipticity α of the exciting pulses, it obtains its maximum with the linear ($\alpha = \pi/4$) orthogonal polarizations of exciting pulses, and it becomes zero with their circular ($\alpha = 0$) orthogonal polarizations. The reason for this result is that in case of circular polarizations of exciting pulses there retains the symmetry with respect to rotations around the direction of pulse propagation (the axis Z), so that the integration over the velocity angles ϕ provides zero result for echo intensity, while in the case of linear polarizations of exciting pulses such symmetry is broken and after the integration over the angles ϕ there remain the nonzero terms providing the echo signal. It also follows from (21) and (22) that in case of linear ($\alpha = \pi/4$) polarizations of exciting pulses the collision-induced echo signal is also linearly polarized along the polarization of the first exciting pulse, while in the general case of elliptically polarized pulses the echo polarization does not coincide with the polarizations of neither the first nor the second exciting pulses.

Let us now compare the amplitude $|e_x^c(\tau)|$ of the collision-induced echo formed by the two linearly orthogonally polarized exciting pulses ($\mathbf{l}_1 = \mathbf{l}_x$, $\mathbf{l}_2 = \mathbf{l}_y$, $\alpha = \pi/4$) and that $|e_x^e(\tau)|$ of the ordinary echo formed by the two collinearly polarized exciting pulses ($\mathbf{l}_1 = \mathbf{l}_2 = \mathbf{l}_x$) at the instant of time $t' = \tau$ when the echo amplitudes obtain their maximums. The assumption $|\lambda| \ll \gamma$ implies that for the time intervals $\tau \leqslant 1/\gamma$ the inequality $|\lambda|\tau \ll 1$ holds true, so that

$$\sinh\left(\frac{\lambda\tau}{2}\right) \approx \frac{\lambda\tau}{2}.$$

Then, as follows from (17), (21), and (22), the difference $|\lambda|$ in the relaxation rates of elastic depolarizing collisions may be obtained from the experimental measurements of the ratio of these amplitudes:

$$|\lambda| = \frac{1}{\tau}\sqrt{8\left|\frac{e_x^c(\tau)}{e_x^e(\tau)}\right| F_c}, \quad (25)$$

where factor

$$F_c = \left|\frac{g(0)}{g_c(0)}\right|$$

is defined by the difference in the shapes (18), (23), and (24) of the ordinary and collision-induced echoes. Generally, the factor F_c depends on the areas θ_n ($n = 1,2$) of the exciting pulses and on the Doppler half-width ku of the spectral line. In case of narrow spectral lines ($kuT_n \ll 1$) it does not depend on the pulse areas and equals $F_c = 15/8$. In case of broad spectral lines ($kuT_n \gg 1$) it also does not depend on the pulse areas and equals $F_c = 1$ if these areas are small enough, so that $\theta_n \ll kuT_n$. The latter is the case realized in our experimental setup.

V. EXPERIMENTAL RESULTS ON COLLISION-INDUCED PHOTON ECHO

A. Experimental setup

The experimental scheme in Fig. 1 shows the excimer XeCl laser (308 nm wavelength, 5–6 ns pulse duration, 20 mJ average pulse energy) used as a pump source for the dye laser operating on a solution of rhodamine 110 and the external optical scheme.

The dye laser consisted of a master oscillator (10-cm cavity shown in Fig. 1 as a broken-line box) and two

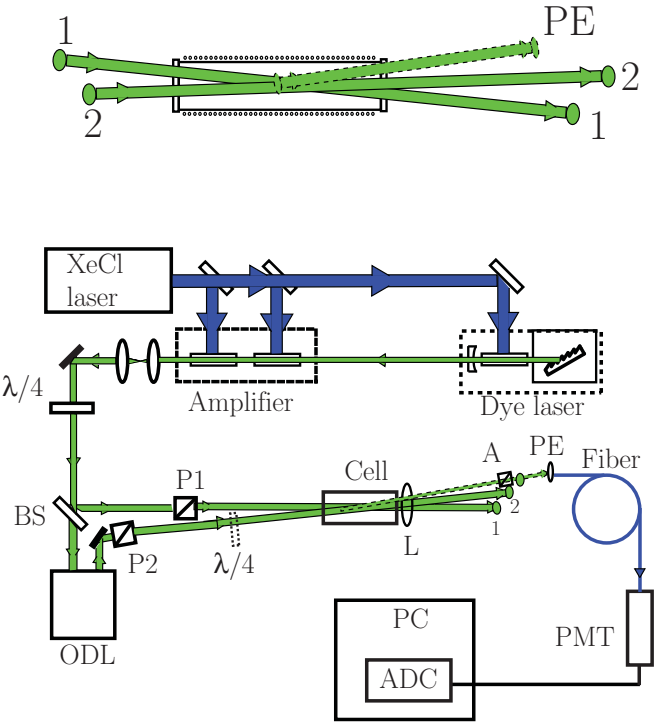

FIG. 1. (Color online) Experimental scheme for investigation of photon-echo polarization. The inset at the top shows the scheme of angular photon echo.

sequential amplification stages. A slow circulation of alcohol dye solution was ensured for the master oscillator and both amplifiers. The master oscillator cavity was formed by 1800 grooves/mm grating, operating in the second diffraction order in the auto-collimation regime and an output dielectric mirror. The grating placed inside a chamber with a controllable dry nitrogen pressure allowed us to make a fine tuning of the master oscillator frequency. An additional 1200 grooves/mm diffraction grating placed at the output of the master oscillator served as spectral selector for the rejection of spontaneous emission of the dye cell. Spatial-angular selectors consisted of two positive lenses with a diaphragm between them, were placed between the master oscillator and the first amplification stage, as well as between the amplification stages. The central part of the beam emerging from the final amplification stage was extracted through the diaphragm of 1.5 mm diameter and expanded by a Kepler telescope up to 10 mm diameter to be delivered to the external optical scheme. The application of spatial-angular selectors and a telescopic beam expander allowed us to reduce the background related to the superluminescence of dye, and to prepare a radiation beam with a sufficiently uniform transverse intensity distribution and with a divergence close to the diffraction limit. The resulting power of dye laser pulse after passing through two amplifiers was 250 μJ; the pulse duration was 2.5–5 ns. A neutral optical filter was placed at dye laser output to control the areas of exciting pulses. The filter transmission of 10% was applied for echo formation in our experimental condition; in such a case the pulses areas were close to the optimal values of $\pi/2$ and π for the first and second pulses, correspondingly. Spectral properties of our dye laser were improved as compared to the previous work [24] by Fabry-Pérot interferometer inserted into the master oscillator between the grating and the dye cell. Now the dye laser pulse spectrum contains only one strong mode with the spectral width less than 100 MHz in 90 cases out of 100. The other 10% of radiation pulses contain two modes with the spectral separation of 1.5 GHz. Optical responses from medium for these 10% of pulses were rejected at a stage of computer processing of registered data.

External optical scheme (see Fig. 1) included beam splitter (BS) and optical delay line (ODL) used to create the pair of coherent exciting pulses and two Glan-Taylor prisms P1 and P2 as independent polarizing elements for each of two exciting pulses. A quarter-wavelength plate (denoted as "$\lambda/4$" in Fig. 1) inserted between the output beam and the BS made it possible to choose the necessary orientation for the polarization plane of each beam by the corresponding orientation of Glan-Taylor prisms. If necessary, linear polarization of any exciting beam (or even both) could be converted into circular polarization using another quarter-wavelength plate (marked as $\lambda/4$ and drawn as broken line plate inserted into the second exciting beam in Fig. 1). The film polarizer A placed after the working cell (Cell in Fig. 1) provided the polarization analysis of photon echo detected by highly sensitive short-time-response photomultiplier (PMT). An additional photodiode (not shown in Fig. 1) was used to control the power of both exciting pulses. All the signals were converted into digital form by the analog-to-digital converter (ADC in Fig. 1) triggered by the first exciting pulse. Data acquisition, averaging, and treatment were done by personal computer (PC).

The scheme of angled photon echo was used for reliable photon echo (PE in Fig. 1) detection as shows an insert at the top of Fig. 1. Part of the beam delayed by an ODL (second pulse of exciting radiation) was directed to the working cell under the angle of about 2×10^{-3} rad to the first pulse. Such a scheme allowed us to detect a signal of photon echo without considerable losses of its amplitude and, simultaneously, without photomultiplier bleaching by the radiation of exciting pulses, due to spatial separation between echo and exciting pulses. The photon-echo signal was focused onto the fiber end (Fiber in Fig. 1) and delivered to the PMT for detection.

The state of polarization for exciting pulses and for the photon echo were analyzed by the detection of polarization diagrams obtained using the analyzer A (see Fig. 1) in front of the PMT.

To suppress the influence of power and spatial distribution instabilities of an excimer laser on the data, several technical solutions were undertaken, including the above-mentioned design of dye laser and external optical scheme, investigation of dye laser radiation properties, and a special technique of data acquisition and treatment (see for details [24,40]).

In this experiment, special attention was paid to the absence of any external stray fields, especially the magnetic ones, in the area of the working cell filled with ytterbium vapors. The magnetic field was measured inside the cold cell without vacuum and its value was not higher than 20 mG. The evaporation of ytterbium was induced by double heating wires passing along the cylindrical cell. This construction allowed us to minimize the stray longitudinal magnetic field from the heater. The absence of any stray magnetic field was finally controlled via the absence of non-Faraday rotation for the photon-echo polarization plane. This could be done with an accuracy of polarizer angle measurement of about 1°; the above-mentioned upper limit for stray magnetic field (if this field was directed strongly along the cell axis) could imply the non-Faraday rotation by an angle of about 1.4° according to our measurements in [24]. Hence, both methods to estimate the stray magnetic field agree.

The temperature of the working cell with ytterbium vapor was kept between 800 and 840 K, which corresponds to Yb pressure 3.9–12.9 mTorr. In order to avoid the undesirable collision effects on the polarization properties of photon echo, the temperature in a working cell was maintained as low as possible; so most of experiments were made at 800 K. The working cell heater was driven by a special autonomic electronic scheme which warranted the temperature stability not worse than ± 2 K.

The sample with a natural content of ytterbium isotopes was used. The exciting radiation wavelength was thoroughly controlled by an electronic wavelength meter in order to get the operation spectral region coinciding with the Doppler center of the ^{174}Yb isotope. The precision of wavelength meter was 10^{-4} nm, which (for the wavelength of ^{174}Yb inter-combination transition under investigation) corresponds to 100 MHz in the frequency scale. Isotopic shifts for natural ytterbium were measured in [41]. The neighboring isotopic lines for ^{174}Yb are ^{176}Yb and ^{172}Yb, which are shifted by -954 MHz and $+1$ GHz, correspondingly. All these even isotopes do not have a hyperfine structure, too. Ytterbium odd

isotopes have higher isotopic shifts and do not overlap with the Doppler width of ^{174}Yb absorption line in our experimental conditions.

The deviation of polarization of exciting pulses from the ideal linear was not greater than 10^{-3} in power. The circular polarization of exciting pulses deviated from the ideal circularity at about 3% . The origin of this inaccuracy of measurements is related to some amplitude instability of dye laser (rhodamine 110) pumped by the excimer laser.

B. Collision-induced echo generated in a mixture of Yb-Xe by two orthogonal linear polarizations pulses

The right part of the Fig. 2 shows the power (in arbitrary units) of collision-induced photon echo generated by two mutually orthogonal linearly polarized exciting pulses of laser radiation resonant to the transition $(6s^2)\,^1S_0 \leftrightarrow (6s6p)\,^3P_1$ of ^{174}Yb in a mixture of Yb + Xe, as a function of Xe pressure. Collision-induced echo is absent at zero buffer gas pressure. As buffer gas pressure grows, collision-induced photon-echo power increases, then reaches its maximum value and starts to decay exponentially in a high pressure limit of buffer gas. This nonmonotonic behavior of collision-induced echo power as a function of buffer gas pressure is in contrast to ordinary (generated in the same gas mixture by pulses of resonant radiation with linear parallel polarizations) echo behavior represented in the left part of Fig. 2. The error bars for echo power shown in both parts of Fig. 2 arose from the statistics of power storage and averaging; the origin of theses errors lies in fluctuations of pulse laser power. The buffer pressure was measured with high accuracy; these errors are less than

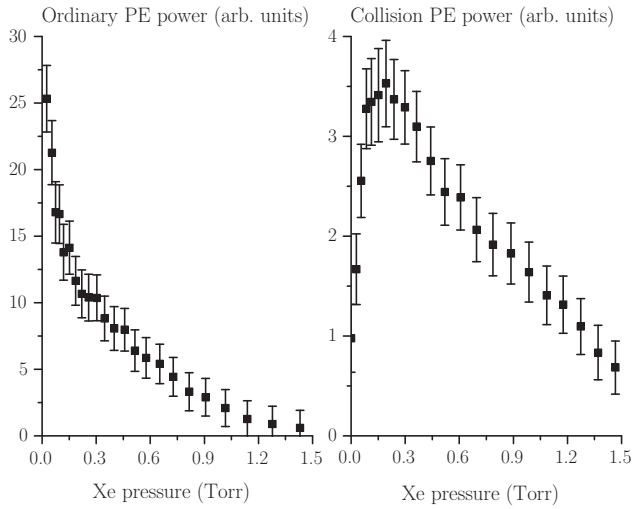

FIG. 2. Buffer gas pressure dependence for ordinary (left) and collision-induced (right) photon echoes generated in a mixture of ^{174}Yb + Xe by resonant exciting pulses of laser radiation with parallel (left) or mutually orthogonal (right) linear polarizations. Error bars for echoes power are related to laser pulses power fluctuations; buffer pressure errors are less than experimental point size. As compared to ordinary echo, the collision-induced echo has several orders of magnitude less power and shows nonmonotonic buffer pressure dependence.

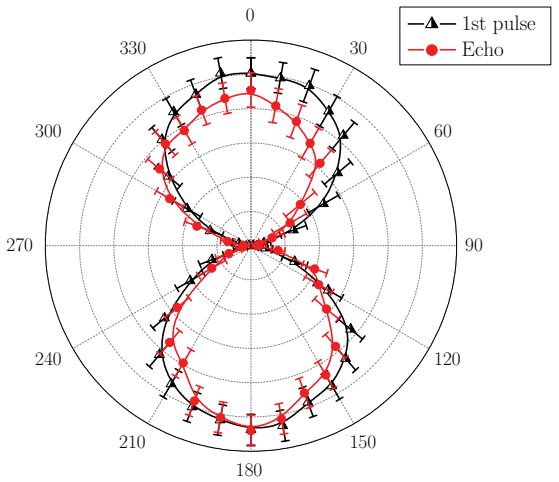

FIG. 3. (Color online) Polarization diagrams for the first exciting pulse (half-filled triangles) and collision-induced photon echo (solid circles). Error bars for exciting pulse power and for collision-induced echo power are related to laser pulse power fluctuations; polarizer angle error is less than experimental point size. Collision-induced photon echo has linear polarization coinciding with the polarization of the first exciting pulse.

experimental points size; that is why the error bars for pressure are not indicated in Fig. 2.

The maximum value of collision-induced echo is reached at Xe pressure of about 200 mTorr, and its value is several orders of magnitude lower than ordinary echo power at the same value of buffer gas pressure. Buffer gas pressure dependence of collision-induced echo and comparison of ordinary and collision-induced echo powers allow us to make a rough estimate of the difference between the above mentioned relaxation constants (see Discussion).

Polarization of collision-induced photon echo generated by two mutually orthogonal linearly polarized exciting pulses of laser radiation resonant to transition $(6s^2)\,^1S_0 \leftrightarrow (6s6p)\,^3P_1$ of ^{174}Yb in a mixture of Yb + Xe was investigated using analyzer A (see Fig. 1). In Fig. 3, the power of collision-induced echo (solid circles) is plotted as a function of rotation angle of analyzer A. The distances from the center of the picture are proportional to the radiation power transmitted by analyzer A at a given rotation angle. Both of these polarization diagrams—for collision-induced photon echo and for the first exciting pulse (half-filled triangles)—are represented in Fig. 3 for comparison. The error bars for echo and exciting pulse power are indicated in both curves; as in the previous experimental result (see Fig. 2), the power errors origin is related to laser pulse power fluctuations. As was already discussed (see Experimental Setup), the polarizer angle measurement accuracy was about 1°; this value is less than experimental points size, so the angle error bars are not shown in Fig. 3.

Unlike ordinary photon echo, which "follows" the polarization of the second exciting pulse, the collision-induced echo polarization coincides with the polarization of the first exciting pulse. This result well agrees with both the earlier prediction [36] and the analytical calculation in the previous section.

C. Opposite circular polarizations of exciting pulses

As was predicted in [37] and experimentally verified in [38], there is another combination of exciting pulses polarizations which gives zero power of ordinary photon echo, opposite circular polarizations. The calculations made in Sec. IV predict that the collision-induced echo cannot be generated at transition $0 \leftrightarrow 1$ even if we take into account depolarizing collisions anisotropy.

In order to verify this "negative" prediction, the sensitivity of collision-induced echo detection was improved in the following way. From the signal detected by PMT at the conditions of resonant excitation at wavelength $\lambda = 555.802$ nm (as measured by λ-meter at the atmospheric pressure), which corresponded to the center of Doppler contour of ^{174}Yb, the signal at nonresonant wavelength of $\lambda = 555.815$ nm was subtracted. This technique permitted the suppression by at least one order of magnitude of a residual stray signal arising from the wings of spatial distribution of exciting pulses. This differential signal is shown in Fig. 4 for two experimental cases: One corresponds to mutually orthogonal linear polarizations of exciting pulses (black curve, right vertical axis), and another one (gray curve, left vertical axis) to the opposite circular polarizations. For the sake of clarity, the black curve and its axis are shifted up.

In Fig. 4, the following signals appear from the left to the right. Two peaks directed down were interpreted as absorption of exciting pulses in a mixture of Yb + Xe; the time delay between them corresponds to 42 ns, which equals the time delay between exciting pulses provided by the ODL. At the tail of the second peak the signal changes its sign to the opposite one. This can be interpreted as the appearance of a free polarization decay signal. All these signals appeared both for linear orthogonal and opposite circular polarizations of exciting pulses. As for the photon-echo signal, it appeared

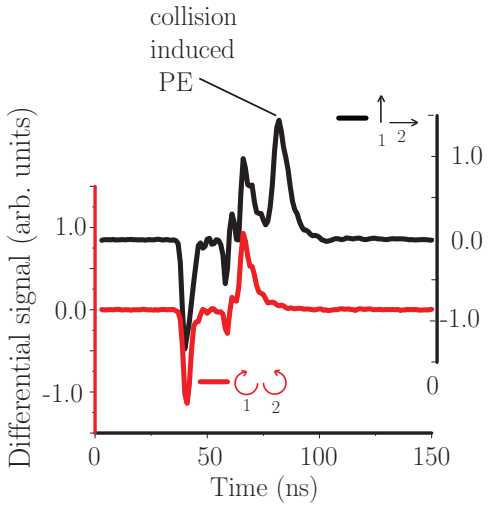

FIG. 4. (Color online) Differential signal detected in a mixture of Yb + Xe for the opposite circular polarizations of exciting pulses (gray curve, left vertical axis) and for linear mutually orthogonal polarizations (black curve, right vertical axis; the curve is shifted up for clarity). Opposite circular polarizations do not generate the collision photon echo, unlike linear orthogonal polarizations of exciting pulses.

only for linear orthogonal polarizations of exciting pulses. It is worth emphasizing that other experimental conditions—pressure of Yb and Xe in a mixture, powers and radial distributions of exciting pulses, time delay between them, a small angle between wave vectors—were identical. The only one difference consisted of the quarter-wave plate inserted in both exciting beams in order to convert linear polarizations into circular ones. As is clear from Fig. 4, the collision echo is detected only for linear orthogonal polarizations of exciting pulses.

VI. DISCUSSION

We assume a linear dependence of relaxation rates Γ_i on buffer gas pressure p in a mixture of ytterbium with rarefied gases $\Gamma_i(v) = c_i(v)p$. As follows from Eq. (21), the collision-induced echo intensity may be written as a function of buffer gas pressure as

$$I_c(p) = I_0 e^{-4ap\tau} p^4, \tag{26}$$

where

$$a = \frac{d\gamma}{dp} = \frac{1}{2}[c_0 + c_1]$$

is constant. I_0 is some normalization constant which does not depend on pressure and can be obtained after the velocity distribution integration. Both I_0 and a are independent on buffer gas pressure. Collision-induced echo reaches its maximal power at buffer pressure $p_m = 1/(a\tau)$. We obtain $p_m = 253$ mTorr as an average value for a set of our experiments for a Yb + Xe mixture. The total error of experimental data was not higher than 15%. So we can estimate $a = (9.41 \pm 1.42) \times 10^7$ s^{-1} Torr^{-1}. The maximum of the difference between relaxation constants Γ_0 and Γ_1 can be estimated via formula (21), where $|\lambda| = |c_0 - c_1|p$ (under the assumption $[\Delta_0(v) - \Delta_1(v)] = 0$). In our experiment the ordinary echo had a 1.7×10^5 times higher power than the collision-induced echo under identical experimental conditions. So we estimate $|c_0 - c_1| \approx 0.14 p_m \tau$. Taking into account the experimental accuracy of 15%, we can get the estimates for $\max\{c_0, c_1\} = (10.1 \pm 1.5) \times 10^7$ s^{-1} Torr^{-1}, while $\min\{c_0, c_1\} = (8.8 \pm 1.3) \times 10^7$ s^{-1} Torr^{-1}. Both values should be considered as upper estimates only. The relative difference between relaxation rates Γ_0 and Γ_1,

$$b = 2\frac{|c_0 - c_1|}{c_0 + c_1},$$

can be estimated more reliably as $b \leqslant 14\%$.

A qualitative ("at fingertips") picture of collision-induced photon echo generated at transition $0 \leftrightarrow 1$ by two pulses of resonant radiation with linear mutually orthogonal polarizations may be sketched as the following sequence of events. After interaction of ytterbium vapor with the first exciting pulse of linear polarization, medium polarization induced by this pulse has the same type of polarization, with the linear one parallel to the polarization vector of the first pulse. There is only one possibility for this polarization vector of the medium to acquire the component parallel to the polarization of the second exciting pulse, and this possibility is due to the anisotropy of relaxation (different relaxation rates for the direction along active atom velocity and in perpendicular

direction); this takes place during the temporal interval after the first and before arrival of the second pulse with orthogonal linear polarization. This would be impossible in the case of isotropic relaxation. The anisotropic collisions "effectively rotate" to dipole moments of individual atoms, depending on their velocity. As a result, medium polarization created by the first exciting pulse acquires an orthogonal component; now it can interact with the second pulse of resonant exciting radiation and obtains the possibility for Doppler rephasing. During the time interval between the second pulse and the collision-induced echo appearance, along with the Doppler rephrasing, the same kind of reverse atomic dipole "effectively rotates" due to collisions takes place so that, at the instance of echo appearance, the atomic dipoles are aligned along the polarization vector of the first radiation pulse, and so the collision-induced photon echo is polarized. For the exciting pulses of opposite circular polarizations there is rotation symmetry around the wave vector of exciting pulses; this symmetry implies zero photon echo after integration over velocity distribution. Such a symmetry is absent for exciting pulses with linear mutually orthogonal polarizations, and nonzero terms for echo amplitude appear after averaging over velocity distribution.

In conclusion, at transition $^1S_0(6s^2) - ^3P_1(6s6p)$ ^{174}Yb (type $0 \leftrightarrow 1$), the photon echo induced by collisions is generated by two pulses of resonant radiation with linear mutually orthogonal polarizations. There is no collision-induced photon echo for opposite circular polarizations of exciting pulses, at least at the level of 0.01 of maximum power corresponding to collision-induced echo generated by two pulses with linear mutually orthogonal polarizations.

The collision-induced photon-echo power shows nonmonotonic dependence on the pressure of heavy atomic buffer (here Xe), and its polarization is linear and coincides with the polarization of the first exciting pulse.

All the experimentally revealed peculiarities of collision-induced photon echo are in qualitative agreement with the calculations made in the frames of depolarizing collisions model accounting for the relaxation matrix dependence on the direction of active atoms velocity.

ACKNOWLEDGMENTS

This research was supported by the Russian Foundation for Basic Research (Grants No. 10-02-00071 and No. 11-02-00141) and by Physical Sciences Department of the Russian Academy of Sciences (Programme "Fundamental Optical Spectroscopy and Its Applications," Grant No. 9.2).

APPENDIX A: THE EVOLUTION OPERATOR

The explicit expression of the evolution operator

$$\hat{S}_n = \exp\left(\frac{i}{2}\hat{\Omega}_n T_n\right),$$

where $\hat{\Omega}_n$ is defined by Eq. (3), may be obtained by means of expansion of the exponent function in Taylor series and with an account of the relations

$$\hat{\Omega}_n^{2k} = \hat{\Omega}_{an}^{2k} + \hat{\Omega}_{bn}^{2k},\ k = 1,2,3,\ldots,$$

$$\hat{\Omega}_{an}^2 = \Delta^2 \hat{P}_a + \left(\frac{2|d|e_n}{\hbar}\right)^2 \hat{g}_n \hat{g}_n^\dagger,$$

$$\hat{\Omega}_{bn}^2 = \Delta^2 \hat{P}_b + \left(\frac{2|d|e_n}{\hbar}\right)^2 \hat{g}_n^\dagger \hat{g}_n.$$

Then the parts $(\hat{S}_n)^{\alpha\beta} = \hat{P}_\alpha \hat{S}_n \hat{P}_\beta, (\alpha,\beta = a,b)$ of the evolution operator $\hat{S}_n$ may be transformed to the expressions

$$(\hat{S}_n)^{aa} = \hat{Q}_{an}\hat{P}_a, \quad (\hat{S}_n)^{bb} = \hat{Q}_{bn}^\dagger \hat{P}_b,$$

$$(\hat{S}_n)^{ab} = i\frac{2|d|e_n}{\hbar}\frac{\sin(\hat{\Omega}_{an}T_n/2)}{\hat{\Omega}_{an}}\hat{g}_n,$$

$$(\hat{S}_n)^{ba} = i\frac{2|d|e_n}{\hbar}\hat{g}_n^\dagger\frac{\sin(\hat{\Omega}_{an}T_n/2)}{\hat{\Omega}_{an}},$$

$$\hat{Q}_{\alpha n} = \cos(\hat{\Omega}_{\alpha n}T_n/2) + i\Delta\frac{\sin(\hat{\Omega}_{\alpha n}T_n/2)}{\hat{\Omega}_{\alpha n}}, \quad \alpha = a,b.$$

In the case of transition $J_a = 0 \to J_b = 1$, as follows from (4), the nonzero matrix elements of the dimensionless electric dipole moment operator $\hat{g}_n = (\hat{\mathbf{g}}\mathbf{l}_n^*)$ are

$$(\hat{g}_n)_{0q}^{ab} = \frac{1}{\sqrt{3}}(l_{n,-q})^*, \tag{A1}$$

where $l_{n,q}$ are the circular components of the unit polarization vector of the nth laser pulse, and the operator $\hat{\Omega}_{an}$ is just proportional to the projector $\hat{P}_a$:

$$\hat{\Omega}_{an} = \Omega_n \hat{P}_a,$$

where

$$\Omega_n = \sqrt{\Delta^2 + \frac{4}{3}\left(\frac{|d|e_n}{\hbar}\right)^2} \tag{A2}$$

is the Rabi frequency, the same for both transitions $m_a = 0 \to m_b = \pm 1$. Defining the area of the nth exciting pulse by the relation

$$\theta_n = \frac{2|d|e_n T_n}{\sqrt{3}\hbar}, \tag{A3}$$

so that

$$\Omega_n T_n = \sqrt{(\Delta T_n)^2 + \theta_n^2},$$

we may write the matrix elements of the evolution operator, which are needed for calculation of the echo field strength, as follows:

$$(\hat{S}_n)_{00}^{aa} = \cos\left(\frac{\Omega_n T_n}{2}\right) + i\frac{\Delta}{\Omega_n}\sin\left(\frac{\Omega_n T_n}{2}\right), \tag{A4}$$

$$(\hat{S}_n)_{0q}^{ab} = i\frac{\theta_n}{\Omega_n T_n}\sin\left(\frac{\Omega_n T_n}{2}\right)(l_{n,-q})^*, \tag{A5}$$

while

$$(\hat{S}_n^\dagger)_{0q}^{ab} = -(\hat{S}_n)_{0q}^{ab}.$$

APPENDIX B: THE RELAXATION MATRIX

The evolution of the nondiagonal density matrix elements in the time intervals between and after the pulses is characterized by the frequency detuning Δ, by the relaxation rate due to the spontaneous radiation $\gamma^{(1)}$, and by the two complex relaxation rates $\Gamma_0(v)+i\Delta_0(v)$ and $\Gamma_1(v)+i\Delta_1(v)$ due to the elastic depolarizing collisions. In the frame of reference, where the axis Z' is directed along the atomic velocity vector $\mathbf{v}$, this evolution is described simply by the exponential factor:

$$\rho'^{ab}_{0q}(t)=\rho'^{ab}_{0q}(0)e^{-[\gamma^{(1)}-i\Delta+\Gamma_q(v)+i\Delta_q(v)]t}, \tag{B1}$$

where $q=0,\pm1$ [$\Gamma_{-1}(v)=\Gamma_1(v)$, $\Delta_{-1}(v)=\Delta_1(v)$]. Since $J_a=0$ and $J_b=1$ the initial density matrix elements $\rho'^{ab}_{0q}(0)$ in this frame of reference may be obtained from their values $\rho^{ab}_{0q}(0)$ in the original frame of reference, where the axis Z is directed along the wave vector of the laser pulses by means of rotation matrices $D^1_{qq'}(0,\theta,\phi,)$ according to the relation:

$$\rho'^{ab}_{0q}(0)=\sum_{q'}D^1_{qq'}(0,\theta,\phi)\rho^{ab}_{0q'}(0), \tag{B2}$$

where θ and ϕ are the spherical angles of the atomic velocity vector $\mathbf{v}$ in the original frame of reference. Now to obtain the density matrix elements $\rho^{ab}_{0q}(t)$ in the original frame of reference at the instant of time t we apply the inverse transformation $D^1_{qq'}(-\phi,-\theta,0)$ to the solution (B1):

$$\rho^{ab}_{0q}(t)=\sum_{q'}D^1_{qq'}(-\phi,-\theta,0)\rho'^{ab}_{0q'}(t). \tag{B3}$$

The explicit expression for the rotation matrix $D^1_{qq'}(\phi,\theta,\phi')$ may be found, for example, in the textbook [42]:

$$D^1_{qq'}(\phi,\theta,\phi')=e^{i(q\phi+q'\phi')}d^1_{qq'}(\theta), \tag{B4}$$

$$\hat{d}^1(\theta)=\begin{pmatrix}\frac{1+\cos(\theta)}{2} & \frac{\sin(\theta)}{\sqrt{2}} & \frac{1-\cos(\theta)}{2}\\ -\frac{\sin(\theta)}{\sqrt{2}} & \cos(\theta) & \frac{\sin(\theta)}{\sqrt{2}}\\ \frac{1-\cos(\theta)}{2} & -\frac{\sin(\theta)}{\sqrt{2}} & \frac{1+\cos(\theta)}{2}\end{pmatrix}. \tag{B5}$$

After the substitution of (B1) and (B2) in (B3) and with an account of (B4) and (B4) the evolution of the density matrix elements $\rho^{ab}_{0q}(t)$ in the original frame of reference may be described by means of relaxation matrix $\hat{R}(t)$:

$$\rho^{ab}_{0q}(t)=e^{-\gamma t+i\delta t}\sum_{q'}R_{qq'}(t)\rho^{ab}_{0q'}(0), \tag{B6}$$

where

$$\gamma=\gamma^{(1)}+\frac{\Gamma_1(v)+\Gamma_0(v)}{2},\quad \delta=\Delta-\frac{\Delta_1(v)+\Delta_0(v)}{2},$$

while

$$R_{qq'}(t)=U_{qq'}(t)e^{i(q'-q)\phi}, \tag{B7}$$

$$\hat{U}(t)=\exp\left(\frac{\lambda t}{2}\right)\hat{1}-\sinh\left(\frac{\lambda t}{2}\right)\hat{\Upsilon}, \tag{B8}$$

$$\lambda=\Gamma_0(v)-\Gamma_1(v)+i[\Delta_0(v)-\Delta_1(v)],$$

$$\hat{\Upsilon}=\begin{pmatrix}\sin^2(\theta) & -\frac{1}{\sqrt{2}}\sin(2\theta) & -\sin^2(\theta)\\ -\frac{1}{\sqrt{2}}\sin(2\theta) & 2\cos^2(\theta) & \frac{1}{\sqrt{2}}\sin(2\theta)\\ -\sin^2(\theta) & \frac{1}{\sqrt{2}}\sin(2\theta) & \sin^2(\theta)\end{pmatrix}.$$

We note that though in the frame of reference with the axis Z' directed along the atomic velocity the resolution matrix is diagonal, in the original frame of reference it contains nonzero nondiagonal elements.

[1] N. A. Kurnit, I. D. Abella, and S. R. Hartmann, Phys. Rev. Lett. **13**, 567 (1964).
[2] M. Scully, M. J. Stephen, and D. C. Burnham, Phys. Rev. **171**, 213 (1968).
[3] V. V. Samartsev, Ukr. Fiz. Zh. **14**, 1045 (1969) [in Russian].
[4] C. K. N. Patel and R. E. Slusher, Phys. Rev. Lett. **20**, 1087 (1968).
[5] O. Guillot-Noël, Ph. Goldner, F. Beaudoux, Y. Le Du, J. Lejay, A. Amari, A. Walther, L. Rippe, and S. Kröll, Phys. Rev. B **79**, 155119 (2009).
[6] N. Christensson, T. Polivka, A. Yartsev, and T. Pullerits, Phys. Rev. B **79**, 245118 (2009).
[7] Yu. G. Vainer, A. V. Naumov, and L. Kador, Phys. Rev. B **77**, 224202 (2008).
[8] D. V. Ledovskikh, N. N. Rubtsova, and V. A. Reshetov, Laser Phys. Lett. **7**, 734 (2010).
[9] K. V. Ivanin, A. V. Leontyev, V. S. Lobkov, and V. V. Samartsev, Laser Phys. Lett. **7**, 583 (2010).
[10] N. N. Rubtsova, V. G. Gol'dort, V. N. Ishchenko, S. A. Kochubei, E. B. Khvorostov, D. V. Ledovskikh, and I. V. Yevseyev, Laser Phys. **20**, 568 (2010).
[11] V. I. Prokhorenko, A. Halpin, and R. J. D. Miller, Opt. Express **17**, 97649 (2009).
[12] N. Sangouard, Ch. Simon, J. Minár, M. Afzelius, T. Chanelière, N. Gisin, J.-L. Le Gouët, H. de Riedmatten, and W. Tittel, Phys. Rev. A **81**, 062333 (2010).
[13] S. A. Moiseev and W. Tittel, Phys. Rev. A **82**, 012309 (2010).
[14] G. M. Safiullin, V. G. Nikiforov, V. S. Lobkov, V. V. Samartsev, and A. V. Leontiev, Laser Phys. Lett. **6**, 746 (2009).
[15] V. V. Samartsev, Laser Phys. **20**, 383 (2010).
[16] L. S. Vasilenko and N. N. Rubtsova, Opt. Spektrosk. **58**, 697 (1985) [in Russian].
[17] L. S. Vasilenko, N. N. Rubtsova, and E. B. Khvorostov, JETP **89**, 24 (1999).
[18] I. V. Yevseyev, V. N. Ishchenko, E. B. Khvorostov, S. A. Kochubei, and N. N. Rubtsova, Laser Phys. Lett. **4**, 524 (2007).
[19] L. S. Vasilenko, N. N. Rubtsova, and E. B. Khvorostov, JETP Lett. **62**, 404 (1995).
[20] N. W. Carlson, L. J. Rothberg, A. G. Yodh, W. R. Babbitt, and T. W. Mossberg, Opt. Lett. **8**, 483 (1983).
[21] R. A. Forber, L. Spinelli, J. E. Thomas, and M. S. Feld, Phys. Rev. Lett. **50**, 331 (1983).

[22] J.-C. Keller and J.-L. Le Gouët, Phys. Rev. Lett. **52**, 2034 (1984).
[23] T. Wang, C. Greiner, J. R. Bochinski, and T. W. Mossberg, Phys. Rev. A **60**, R757 (1999).
[24] N. N. Rubtsova, V. N. Ishchenko, E. B. Khvorostov, S. A. Kochubei, V. A. Reshetov, and I. V. Yevseyev, Phys. Rev. A **70**, 023403 (2004).
[25] P. W. Anderson, Phys. Rev. **76**, 647 (1949).
[26] P. W. Anderson, Phys. Rev. **80**, 511 (1950).
[27] S. D. Grossman, A. Schenzle, and R. G. Brewer, Phys. Rev. Lett. **38**, 275 (1977).
[28] L. S. Vasilenko, N. N. Rubtsova, and V. P. Chebotayev, JETP Lett. **38**, 474 (1983).
[29] S. G. Rautian, A. G. Rudavets, and A. M. Shalagin, JETP **51**, 274 (1980).
[30] V. A. Alekseyev and A. V. Malyugin, ZhETF **74**, 911 (1978) [in Russian].
[31] V. A. Alekseyev, T. L. Andreyeva, and A. V. Malyugin, Sov. J. Quantum Electron. **11**, 766 (1981).
[32] V. N. Rebane, Opt. Spektrosk. **24**, 309 (1968) [in Russian].
[33] V. N. Rebane, Opt. Spektrosk. **26**, 673 (1969) [in Russian].
[34] V. M. Yermachenko, Laser Phys. **1**, 129 (1991).
[35] M. P. Chaika, *Interference of Degenerated Atomic States* (Leningrad University Publishing, Leningrad, 1975) [in Russian].
[36] V. K. Matskevich, I. V. Yevseyev, and V. M. Yermachenko, Opt. Spektrosk. **45**, 17 (1978) [in Russian].
[37] A. I. Alekseyev and I. V. Yevseyev, ZhETF **56**, 2118 (1969) [in Russian].
[38] E. B. Khvorostov, V. G. Gol'dort, V. N. Ishchenko, S. A. Kochubei, N. N. Rubtsova, V. D. Salakhutdinov, and I. V. Yevseyev, Laser Phys. Lett. **8**, 290 (2011).
[39] I. V. Yevseyev, V. M. Yermachenko, and V. V. Samartsev, *Depolarizing Collisions in Nonlinear Electrodynamics* (CRC Press, Boca Raton, London, New York, Washington, DC, 2004).
[40] N. N. Rubtsova, V. G. Gol'dort, I. V. Yevseyev, V. N. Ishchenko, S. A. Kochubei, and E. B. Khvorostov, JETP Lett. **87**, 103 (2008).
[41] W. A. van Wijkngaarden and J. Li, J. Opt. Soc. Am. B **11**, 2163 (1994).
[42] A. Messiah, *Mecanique Quantique*, Vol. 2 (Dunod, Paris, 1972).